



Wind turbines and
Doppler weather
radars

L. Norin

This discussion paper is/has been under review for the journal Atmospheric Measurement Techniques (AMT). Please refer to the corresponding final paper in AMT if available.

A quantitative analysis of the impact of wind turbines on operational Doppler weather radar data

L. Norin

Atmospheric Remote Sensing, Research and Development, Swedish Meteorological and Hydrological Institute, Norrköping, Sweden

Received: 26 July 2014 – Accepted: 18 August 2014 – Published: 27 August 2014

Correspondence to: L. Norin (lars.norin@smhi.se)

Published by Copernicus Publications on behalf of the European Geosciences Union.

Title Page

Abstract

Introduction

Conclusions

References

Tables

Figures



Back

Close

Full Screen / Esc

Printer-friendly Version

Interactive Discussion



Abstract

In many countries wind turbines are rapidly growing in numbers as the demand for energy from renewable sources increases. The continued deployment of wind turbines can, however, be problematic for many radar systems, which are easily disturbed by turbines located in radar line-of-sight. Wind turbines situated in the vicinity of Doppler weather radars can lead to erroneous precipitation estimates as well as to inaccurate wind- and turbulence measurements. This paper presents a quantitative analysis of the impact of a wind farm, located in southeastern Sweden, on measurements from a nearby Doppler weather radar. The analysis is based on six years of operational radar data. In order to evaluate the impact of the wind farm, average values of all three spectral moments (the radar reflectivity factor, absolute radial velocity, and spectrum width) of the nearby Doppler weather radar were calculated, using data before and after the construction of the wind farm. It is shown that all spectral moments, from a large area at and downrange from the wind farm, were impacted by the wind turbines. It was also found that data from radar cells far above the wind farm (near 3 km altitude) were affected by the wind farm. We show that this is partly explained by changes in the atmospheric refractive index, bending the radar beams closer to the ground. In a detailed analysis, using data from a single radar cell, frequency distributions of all spectral moments were used to study the competition between the weather signal and wind turbine clutter. We show that when weather echoes give rise to higher reflectivity values than that of the wind farm, the negative impact of the wind turbines disappears for all spectral moments.

1 Introduction

As a response to the increasing demand for renewable energy the number of wind turbines is growing rapidly in many countries around the world. The worldwide installed cumulative energy capacity of wind turbines has shown a more than 13-fold increase

AMTD

7, 8743–8776, 2014

Wind turbines and Doppler weather radars

L. Norin

Title Page

Abstract

Introduction

Conclusions

References

Tables

Figures



Back

Close

Full Screen / Esc

Printer-friendly Version

Interactive Discussion



Wind turbines and Doppler weather radars

L. Norin

Title Page

Abstract

Introduction

Conclusions

References

Tables

Figures



Back

Close

Full Screen / Esc

Printer-friendly Version

Interactive Discussion



during 2001–2013. In Sweden, the wind power capacity has increased even more, 15 times, during the same period (Global Wind Energy Council, 2014). In the coming years many more wind turbines are expected to be built and existing, older ones are likely to be replaced by larger, next generation, turbines. Modern wind turbines are large structures, many reaching 150 m above the ground. Clusters of densely spaced wind turbines, so called wind farms, are being built both on- and offshore.

The continued deployment of wind turbines and wind farms presents a problem for many radar systems, which are easily disturbed by wind turbines located in radar line-of-sight. Due to their rotating blades, interference caused by wind turbines is more severe for radar systems than interference caused by stationary structures (e.g. masts or towers). Many Doppler radars use a clutter filter that suppresses echoes originating from objects with no or little radial velocity but such filters do not work for moving objects such as the rotating blades of a wind turbine. It has been shown that wind turbines located in line-of-sight of Doppler radars can have a detrimental impact on the performance of both military- and civilian radar systems (see, e.g., Poupart, 2003; Department of Defense, 2006; Lemmon et al., 2008; Lute and Wieserman, 2011).

Doppler weather radars, employed by meteorological and hydrological services, can also be negatively affected by nearby wind turbines. Weather radars are valuable tools for monitoring precipitation and wind shear as well as to observe hazardous events such as hailstorms, heavy rainfall, and tornadoes. Information from weather radars is also used as input to numerical weather prediction- and flood forecasting models. Errors in weather radar data may propagate to affect the output of such forecast systems (Rossa et al., 2011).

Several studies dedicated to wind turbine impact on weather radar data have presented images of radar composites that convincingly show that wind farms indeed can be detected by weather radars (see, e.g., Burgess et al., 2008; Crum and Ciardi, 2010; Vogt et al., 2011). In other studies, time series of raw radar data have been recorded in order to perform detailed analyses of the impact of wind turbines by spectral analysis. Gallardo et al. (2008) collected raw radar data during a few months from a Spanish

Wind turbines and Doppler weather radars

L. Norin

Title Page

Abstract

Introduction

Conclusions

References

Tables

Figures



Back

Close

Full Screen / Esc

Printer-friendly Version

Interactive Discussion



C-band weather radar to analyse the impact of a large wind farm while Isom et al. (2009) used several hours worth of raw data from two US S-band weather radars to investigate the same phenomenon. Toth et al. (2011) used a mobile X-band Doppler radar to study the impact of wind turbines from close range. However, only a few analyses of wind turbine impact on long time series of operational radar data have been published (Haase et al., 2010; Norin and Haase, 2012).

The main objective of this study is to analyse the impact of wind turbines on operational Doppler weather radar volume data. This study thus extends the work by Haase et al. (2010) and Norin and Haase (2012). In this study the wind turbine impact on all three spectral moments (the radar reflectivity factor, radial velocity, and spectrum width) have been investigated in order to improve the understanding of wind turbine impact on Doppler weather radar data. In total, six years worth of operational polar volume data were used for the data analysis.

The structure of the paper is as follows. The technical characteristics of the Swedish radars are described in Sect. 2. The radar data set together with the analysed wind farm are presented in Sect. 3. In Sect. 4.1 we show the impact of wind turbines on data from a single radar scan by comparing average values of the spectral moments, before and after the construction of the wind farm. In Sect. 4.2 the wind turbine impact on polar volume data is investigated. Section 4.3 presents a detailed analysis of the wind turbine impact on data from a single radar cell, by examining frequency distributions for all spectral moments as a function of reflectivity from a reference radar cell. The competition between the weather signal and wind turbine clutter is investigated in Sect. 4.4 and, finally, in Sect. 5, a summary of the study is given and conclusions of the analyses are drawn.

2 The Swedish weather radars

The Swedish weather radar network consists of 12 horizontally polarized Ericsson C-band Doppler radars, providing almost complete national coverage. The radars perform

azimuthal scans of 360° around a vertical axis for 10 tilt angles, θ , ranging from $\theta = 0.5^\circ$ to $\theta = 40^\circ$. Together, these scans make up polar volume data sets which are provided with an update time of 15 min.

The data processing is managed by the radar signal processor and data are output in matrices consisting of 120×420 radar cells for every scan. The range resolution of each radar cell is 2 km for the four lowest tilt angles and 1 km for the others, the azimuthal resolution is $360/420 \approx 0.86^\circ$ for all scans. The main radar lobe has a half-power beam width of 0.9° .

Doppler weather radars measure three spectral moments (see, e.g., Doviak and Zrnić, 2006): the radar reflectivity factor (hereafter referred to as reflectivity), radial velocity, and spectrum width. These spectral moments are used to estimate quantities such as precipitation rate, wind speed, and turbulence.

Reflectivity, Z , is the power of the returned signal and is measured by the radar in units of dBZ. The Swedish weather radars have a dynamic range of > 85 dB and measures Z between -30 dBZ and 71.6 dBZ in steps of 0.4 dBZ. The minimum value (-30 dBZ) represents all measurements ranging from $-\infty$ dBZ to -30 dBZ. Such values are classified as undetected measurements.

Radial velocity, V , is obtained as the first moment of the power-normalised Doppler spectrum. Two pulse repetition frequencies (PRFs) are used alternatively to allow real-time dealiasing of the radial velocities. The maximum unambiguous velocity is $\pm 24 \text{ m s}^{-1}$ for the four lowest scans and $\pm 48 \text{ m s}^{-1}$ for the six highest scans. The radial velocity resolution is 0.1875 m s^{-1} (0.375 m s^{-1} for the higher scans). Undetected reflectivity measurements ($Z \leq -30$ dBZ) result in unreliable estimates of radial velocity and such measurements are therefore classified as undetected.

Spectrum width, W , is calculated as the square root of the second moment about the first of the power-normalised spectrum. The measurements of the spectrum width fall into one of four classes: 0–1, 1–2, 2–3, and $> 3 \text{ m s}^{-1}$ for the four lowest scans and 0–2, 2–4, 4–6, and $> 6 \text{ m s}^{-1}$ for the six highest scans. As for radial velocity,

Wind turbines and Doppler weather radars

L. Norin

Title Page

Abstract

Introduction

Conclusions

References

Tables

Figures



Back

Close

Full Screen / Esc

Printer-friendly Version

Interactive Discussion



have a rotor diameter of 100 m, a cut-in wind speed of 3.5 m s^{-1} and a cut-out wind speed of 25 m s^{-1} .

The wind turbines were erected in October and November 2009 and the wind farm became operational in April 2010. The proximity of the Brunsmo wind farm to weather radar Karlskrona together with the date of the wind farm's start-of-operations (near the middle of the homogeneous radar data set) makes Brunsmo wind farm well suited for a detailed study.

Figure 1 shows a schematic picture of the locations and heights of the wind turbines of the Brunsmo wind farm together with the altitudes of the radar lobes' half-power beam width for the five lowest tilt angles (0.5° , 1.0° , 1.5° , 2.0° , and 2.5°) at the wind farm, assuming standard propagation conditions. From Fig. 1 it is seen that all wind turbines are in radar line-of-sight for the scans with the two lowest tilt angles ($\theta = 0.5^\circ$ and $\theta = 1.0^\circ$). Three of the five wind turbines are located within the same radar cell (azimuth gate 52, near 44° azimuth).

4 Methods and results

4.1 Wind turbine impact on a single radar scan

One way to investigate the impact of wind turbines on Doppler weather radar data is to compare the average values of the spectral moments before and after the construction of a wind turbine. The differences between these average values provide an estimate of the impact of the wind turbine.

Reflectivity, Z , and spectrum width, W , are well suited for calculating average values but radial velocity measurements, V , can be both positive and negative, depending on the wind direction relative to the radar. Since we are interested in finding an estimate of the wind turbine impact on V the influence of the wind direction was minimised by studying the absolute radial velocity, $|V|$.

Wind turbines and Doppler weather radars

L. Norin

Title Page

Abstract

Introduction

Conclusions

References

Tables

Figures



Back

Close

Full Screen / Esc

Printer-friendly Version

Interactive Discussion



wind farm led to spectral width being detected more often. The relative frequency of occurrence of W increased from approximately 50% to more than 90%, at and behind the wind turbines.

Together, Figs. 2 and 3 show that the construction of the Brunsmo wind farm has led to real (detected) measurements of all spectral moments to occur more frequently. The average value of Z increased at and near the wind turbines whereas $\langle|V|\rangle$ and $\langle W\rangle$ increased in radar cells located at the wind turbines but decreased behind.

4.2 Wind turbine impact on polar volume data

As was shown in Fig. 1 the wind turbines in Brunsmo wind farm are in radar line-of-sight for the scans with the two lowest tilt angles ($\theta = 0.5^\circ$ and $\theta = 1.0^\circ$). However, this calculation is based on the assumption of standard atmospheric conditions and further assumes that the extent of the radar lobe is limited by its half-power beam width. In order to investigate whether scans with higher tilt angles also are affected by the Brunsmo wind farm, data from all 10 scans in the polar volume were analysed.

Figure 4 shows the impact of the wind farm on $\langle Z\rangle$, $\langle|V|\rangle$, and $\langle W\rangle$ for all 10 scans in the polar volume. In Fig. 4 every scan is represented by the radar cells in the range bin in which the wind turbines would be located if a vertical line from the turbines was drawn from the ground. For the higher tilt angles ($2.5^\circ \leq \theta \leq 40^\circ$) the average values of the spectral moments from the two range bins nearest to the wind turbines were used, since for these scans the range resolution is two times that of the lower scans (cf. Table 1). Furthermore, in order to clearly display the change in the spectral moments for all scans in the same figure the mean value in azimuth (for the extent of the analysed area, $35\text{--}53^\circ$) for every spectral moment from before the construction of the wind farm, were subtracted from the measurements (both before and after the construction of the wind farm). These mean values are denoted by Z_0 , V_0 , and W_0 , respectively.

Figure 4a and b shows $\langle Z\rangle - Z_0$ before and after the construction of the wind farm, respectively. Figure 4a shows that before the wind farm was built $\langle Z\rangle - Z_0$ was homogeneous in azimuth for all scans. In Fig. 4b, after the construction of the wind farm, an

Wind turbines and Doppler weather radars

L. Norin

Title Page

Abstract

Introduction

Conclusions

References

Tables

Figures



Back

Close

Full Screen / Esc

Printer-friendly Version

Interactive Discussion



Wind turbines and Doppler weather radars

L. Norin

Title Page

Abstract

Introduction

Conclusions

References

Tables

Figures



Back

Close

Full Screen / Esc

Printer-friendly Version

Interactive Discussion



by the wind farm. Here we have investigated a third possibility, that the impact could be due to anomalous propagation, i.e. bending of the radar beam due to changes in the atmospheric refractive index. Anomalous propagation can sometimes result in scattering from objects on the ground, not normally seen by the radar. Such propagation conditions can be caused by temperature inversions or by a rapid decrease in water vapour content with height (see, e.g., Patterson, 2008). Temperature inversions can exist at any time of the day in Sweden during the cool season (Devasthale and Thomas, 2012) whereas such inversions most commonly occur in early morning during the warm season. A rapid decrease in water vapour content with height can occur during afternoons in summer (Bodine et al., 2011).

In order to investigate the effect of anomalous propagation, the data presented in Fig. 4 were divided into hourly and seasonally averages. Data for $\langle Z \rangle - Z_0$, $\langle |V| \rangle - V_0$, and $\langle W \rangle - W_0$ from the radar cell in which three wind turbines are located, from all tilt angles, as a function of time of day and season are shown Fig. 6. From Fig. 6a, e, and i it is seen that during winter (December, January, and February, DJF) the impact on the spectral moments is high, regardless of the time of day. During the warm season, especially during summer (June, July, and August, JJA), high impacts on the spectral moments are concentrated to early morning and late afternoon. This effect is most pronounced for scans with low tilt angles and cannot be seen for scans with tilt angles $\theta > 14^\circ$. For radial velocity it can be noted that the largest impact, resulting in a decrease in $|V|$ for higher tilt angles, primarily occur during autumn (September, October, and November, SON).

For the Brunsmo wind farm it is clear that anomalous propagation conditions affects the size of the impact of the wind turbines. Higher impacts are seen when anomalous propagation conditions are common. However, it is still possible that part of the increased levels of the spectral moments can be explained by the radar sidelobes or by scattering from dust or turbulence above the wind farm.

4.3 Wind turbine impact on a single radar cell

In Sects. 4.1 and 4.2 average values of the spectral moments were compared before and after the construction of Brunsmo wind farm. While this is a robust and simple way to illustrate the impact of wind turbines on weather radar data these average values do not separate the weather signal from the unwanted wind turbine clutter. Hence, this method tacitly assumes that the weather signal, on average, was similar during the two measurement periods (before and after the construction of the wind farm).

In order to perform a more in-depth analysis of the impact of wind turbines on radar data one would ideally want to know the actual, unaffected values of the weather signal at all times. A way to simulate this is to use simultaneous measurements from a reference radar cell, a radar cell unaffected by the wind turbines.

This technique was used by Haase et al. (2010) and Norin and Haase (2012) in their works. As reference cells they used radar cells with the same range bin and azimuth gate as the wind turbine-affected radar cells, but from a scan with a higher tilt angle ($\theta = 2.0^\circ$). Furthermore, in order to remove the influence of weather they chose to select only those measurements for which the reflectivity in the reference cell was undetected (i.e. $Z_{\text{ref}} = -30$ dBZ). As can be seen from Fig. 4, such a choice of reference radar cells must be treated with caution since radar cells in scans from higher tilt angles may also be affected by the presence of the wind farm.

In this work a different choice of reference radar cell was used: the radar cells one range bin up-range from the radar cells in which the wind turbines are located. From Fig. 2 it is seen that these radar cells are not affected by the wind farm.

In order to investigate the impact of wind turbines on a single radar cell, we chose to study data from the radar cell in which three wind turbines are located ($\theta = 0.5^\circ$, range bin 7, azimuth gate 52). The corresponding reference radar cell was selected from the scan with the same tilt angle and azimuth gate but one range bin up-range from the wind turbine-affected cell ($\theta = 0.5^\circ$, range bin 6, azimuth gate 52).

Wind turbines and Doppler weather radars

L. Norin

Title Page

Abstract

Introduction

Conclusions

References

Tables

Figures



Back

Close

Full Screen / Esc

Printer-friendly Version

Interactive Discussion



Wind turbines and Doppler weather radars

L. Norin

Title Page

Abstract

Introduction

Conclusions

References

Tables

Figures



Back

Close

Full Screen / Esc

Printer-friendly Version

Interactive Discussion



In the analysis frequency distributions of the spectral moments (Z , V , and W) were examined as functions of Z_{ref} . In order to have sufficiently many samples for the analysis, data for Z and V were sorted into 35 bins.

For Z , one bin was used to count all measurement for which $Z = -30$ dBZ (undetected measurements) and one bin counted all invalid measurements. The remaining 33 bins were equally spaced from $Z = -29.6$ dBZ to $Z = 71.6$ dBZ. For V , one bin was used to count all undetected measurements and one bin counted all invalid measurements. The remaining 33 bins were equally spaced from $V = -24$ m s⁻¹ to $V = 24$ m s⁻¹.

Since measurements of W only consists of four different classes (see Sect. 2) and has separate representations for undetected and invalid measurements, data for W were used as they are.

Let us first examine the validity of the choice of reference radar cell. Figure 7 shows relative frequency distributions of reflectivity from the reference cell, Z_{ref} , and from the wind turbine-affected radar cell, Z_{wt} , before and after the construction of the Brunsmo wind farm, using data from the scan with the lowest tilt angle ($\theta = 0.5^\circ$). From Fig. 7 it is seen that the distributions of Z_{ref} , both before and after the construction of the wind farm, are similar to the distribution of Z_{wt} from before the wind farm was built. Some small differences exist between these distributions but they are minor when compared to the distribution of the Z_{wt} after the construction of the wind farm, which is dominated by a prominent peak near $Z \approx 5$ dBZ.

From Fig. 7 it is seen that neither Z_{ref} nor Z_{wt} are normally distributed. This means that the average value of Z , used in Sect. 4.1 and Sect. 4.2, does not coincide with the value of Z at the peak of the frequency distribution.

Distributions of reflectivity from scans with higher tilt angles, using the same choice for reference radar cells (the radar cells one range bin up-range from the wind turbine-affected cells), all show similar behaviour. The chosen reference radar cells were therefore judged to provide a good (albeit not perfect) representation of the weather signal in the wind turbine-affected radar cells.

Wind turbines and Doppler weather radars

L. Norin

Title Page

Abstract

Introduction

Conclusions

References

Tables

Figures



Back

Close

Full Screen / Esc

Printer-friendly Version

Interactive Discussion



correlation between V_{wt} and V_{ref} , except for $V_{ref} \lesssim \pm 3 \text{ m s}^{-1}$. (It is interesting to note that the cut-in speed of the wind turbines is 3.5 m s^{-1} (see Sect. 3), which could explain the correlation for $V_{ref} \lesssim \pm 3 \text{ m s}^{-1}$.) In Fig. 9d the correlation between V_{wt} and V_{ref} is seen to increase for $-10 \text{ dBZ} \geq Z_{ref} < 5 \text{ dBZ}$, and for $Z_{ref} \geq 5 \text{ dBZ}$, shown in Fig. 9f, it is as strong as before the construction of the wind farm.

As was shown in Fig. 8, a recovery of all spectral moments occurs for increasing values of Z_{ref} . A way to quantitatively analyse this recovery is to calculate the correlation coefficient between the distributions of the spectral moments before and after the construction of the wind farm, as a function of Z_{ref} . This analysis was performed for all 10 scans in the polar volume. The wind turbine-affected radar cells were represented by the radar cells with azimuth gate 52 and the range bin in which the wind turbines would be located if a vertical line was drawn from the ground. The corresponding reference cells were selected from the same azimuth gate but one range bin closer to the radar (cf. Sect. 4.3). Correlation coefficients were only calculated for distributions for which more than 300 measurements existed. The results of the analyses for the three spectral moments (Z , V , and W) for all 10 scans in the polar volume are shown in Fig. 10.

Figure 10a shows the correlation coefficient, ρ , between the distribution of Z at the wind turbines, before ($Z_{wt \text{ bef}}$) and after ($Z_{wt \text{ aft}}$) the construction of the wind farm, as a function of Z_{ref} , for all scans in the polar volume. The correlation coefficient, $\rho(Z_{wt \text{ bef}}, Z_{wt \text{ aft}})$, is seen to increase for increasing values of Z_{ref} (i.e. for increasing influence of the weather signal) and also for higher tilt angles (i.e. for decreasing influence of the wind farm). However, for $Z_{ref} < -5 \text{ dBZ}$ the correlation coefficient for the fifth scan ($\theta = 2.5^\circ$, the lowest scan using the higher radial resolution) is lower than for two scans with lower tilt angles ($\theta = 1.5^\circ$ and $\theta = 2.0^\circ$). This is most likely because these scans use a lower radial resolution (cf. Sect. 2). That the fifth scan is more affected by the wind farm than some of the lower scans can also be seen in Figs. 4 and 5, as well as in Fig. S1 in the Supplement.

Wind turbines and Doppler weather radars

L. Norin

Title Page

Abstract

Introduction

Conclusions

References

Tables

Figures



Back

Close

Full Screen / Esc

Printer-friendly Version

Interactive Discussion



Figure 10b shows the correlation coefficient, ρ , between the distribution of V at the wind turbines, before ($V_{wt\text{ bef}}$) and after ($V_{wt\text{ aft}}$) the construction of the wind farm, as a function of Z_{ref} , for all scans in the polar volume. In Fig. 10b it is again seen that the correlation coefficient, $\rho(V_{wt\text{ bef}}, V_{wt\text{ aft}})$, increases for increasing values of Z_{ref} as well as for higher tilt angles. However, the use a higher radial resolution ($\theta \geq 2.5^\circ$) seems to have a smaller negative impact on the recovery of V_{wt} than for Z_{wt} .

Figure 10c shows the correlation coefficient, ρ , between the distribution of W at the wind turbines, before ($W_{wt\text{ bef}}$) and after ($W_{wt\text{ aft}}$) the construction of the wind farm, as a function of Z_{ref} , for all scan in the polar volume. As for Z and V , the correlation coefficient for W , $\rho(W_{wt\text{ bef}}, W_{wt\text{ aft}})$, increases for increasing values of Z_{ref} and also for higher tilt angles. For the scans with the lowest tilt angle ($\theta = 0.5^\circ$) a correlation greater than 0.9 is only achieved for $Z_{ref} > 15$ dBZ. Since W is limited to four classes (see Sect. 2), fewer values of the correlation coefficient are statistically significant compared to the other spectral moments.

5 Summary and conclusions

Wind turbines located in the vicinity of a Doppler weather radar can have a detrimental impact on the radar's performance. The objective of this study was to investigate the impact of wind turbines on operational Doppler weather radar data. Doppler weather radars measure three spectral moments: the radar reflectivity factor, Z , radial velocity, V , and spectrum width, W . In this work we have analysed the impact of wind turbines on all spectral moments, using two different approaches.

First, the average values for the three spectral moments (reflectivity, $\langle Z \rangle$, absolute radial velocity, $\langle |V| \rangle$, and spectrum width, $\langle W \rangle$) were computed. In this study these averages were calculated using operational radar data from long periods of time before (approximately 2.5 years) and after (approximately 3.5 years) the construction of a wind farm near radar Karlskrona in southeastern Sweden. By comparing the average values before and after, the impact of the wind farm on all spectral moments was

Wind turbines and Doppler weather radars

L. Norin

Title Page

Abstract

Introduction

Conclusions

References

Tables

Figures



Back

Close

Full Screen / Esc

Printer-friendly Version

Interactive Discussion



estimated. For the wind farm studied in this work the average values of the spectral moments in the radar cells in which wind turbines are located, from the scan with the lowest tilt angle, were shown to change after the wind turbines were built; reflectivity increased from $\langle Z \rangle \approx -18$ dBZ to $\langle Z \rangle \approx -6$ dBZ, the absolute radial velocity increased from $\langle |V| \rangle \approx 6$ m s⁻¹ to $\langle |V| \rangle > 8.5$ m s⁻¹, and the spectrum width increased from $\langle W \rangle \approx 2.0$ m s⁻¹ to $\langle W \rangle > 2.5$ m s⁻¹. However, not only those radar cells in which the wind turbines are located were affected by the presence of the wind farm. Several radar cells both cross- and downrange were also affected.

Downrange from the wind turbines tails with increased values of $\langle Z \rangle$ were seen, visible for more than 20 km behind the turbines. This is believed to be caused by multiple scattering of the radar signal between rotor blades and the ground. For $\langle |V| \rangle$ and $\langle W \rangle$, tails with decreased values were observed.

In addition to the changes in values of all spectral moments in data from the scan with the lowest tilt angle it was shown that data from scans with higher tilt angles, far above the wind farm were also affected. Increased values in $\langle Z \rangle$ and $\langle W \rangle$, and decreased values in $\langle |V| \rangle$ were seen up to three kilometres above the wind farm.

That a wind farm can have an impact on radar data at altitudes far above the wind turbines can be due to several reasons. Wind farms not in line-of-sight of a radar can still be detected by the radar's sidelobes. Scattering off dust and turbulence above the wind farm is also a conceivable explanation for changed values in the spectral moments. In this work we investigated the influence of anomalous propagation, i.e. bending of the radar beam due to changes in the atmospheric refractive index. It was shown that increased values in all spectral moment intensified during winter (regardless of the time of day) as well as during early morning and afternoon in the summer, consistent with times when anomalous propagation conditions that bend the radar beam toward the ground are known to occur more frequently.

One of the problems with wind turbine clutter is that their impact on the spectral moments is similar to that of real weather signals. To analyse the competition between the weather signal and wind turbine clutter a second approach, using data from reference

Wind turbines and Doppler weather radars

L. Norin

Title Page

Abstract

Introduction

Conclusions

References

Tables

Figures



Back

Close

Full Screen / Esc

Printer-friendly Version

Interactive Discussion



radar cells, was used. Ideally, data from a reference radar cell should, for any given measurement, show what the unaffected weather signal should be in the wind turbine-affected radar cell. In this work the reference cells were chosen as the radar cells one range bin up-range from the affected radar cells. Data from all three spectral moments, before and after the construction of the wind farm, were then visualised using relative frequency distributions of the spectral moment under study, as a function of Z_{ref} .

The results using this method revealed that all spectral moments from wind turbine-affected radar cells recover their true value (i.e. the value of the weather signal) for increasing values of Z_{ref} . When precipitation gives rise to reflectivity values stronger than those caused by the wind turbines, the negative impact of the wind turbines disappears for all spectral moments.

These results suggest that the weather information from wind turbine-affected radar cells is not always lost. One way to mitigate the impact of wind turbines could be to create conditional filters. If reflectivity from a wind turbine-affected radar cell is larger than that on average caused by the wind turbine, the radar data could still be used. However, when the reflectivity is similar or lower than the average reflectivity caused by the wind turbine, caution should be applied when using radar data from any spectral moment from the wind turbine-affected radar cells.

The Supplement related to this article is available online at doi:10.5194/amtd-7-8743-2014-supplement.

Acknowledgements. This work was financed by the Swedish Energy Agency, under the project VINDRAD+.

Wind turbines and Doppler weather radars

L. Norin

Title Page

Abstract

Introduction

Conclusions

References

Tables

Figures



Back

Close

Full Screen / Esc

Printer-friendly Version

Interactive Discussion



- Kong, F.: Wind Turbine Clutter in Weather Radar: Characterization and Mitigation, Ph.D. thesis, University of Oklahoma, Norman, OK, United States, 2014. 8750
- Lemmon, J. J., Carroll, J. E., Sanders, F. H., and Turner, D.: Assessment of the Effects of Wind Turbines on Air Traffic Control Radars, Tech. Rep. TR-08-454, US Department of Commerce, National Telecommunications & Information Administration, 2008. 8745
- Lute, C. and Wieserman, W.: ASR-11 radar performance assessment over a wind turbine farm, in: Proceedings of the 2011 IEEE Radar Conference, Kansas City, MO, United States, 226–230, IEEE, 2011. 8745
- Norin, L. and Haase, G.: Doppler weather radars and wind turbines, in: Doppler Radar Observations – Weather Radar, Wind Profiler, Ionospheric Radar, and Other Advanced Applications, edited by: Bech, J. and Chau, J. L., InTech, Croatia, doi:10.5772/39029, 2012. 8746, 8750, 8756
- Patterson, W. L.: The propagation factor, F_p , in the radar equation, in: Radar Handbook, 3rd Edn., edited by: Skolnik, M., McGraw-Hill, United States, 2008. 8755
- Poupart, G. J.: Wind Farms Impact on Radar Aviation Interests, Tech. Rep. FES W/14/00614/00/REP, DTI PUB URN 03/1294, QinetiQ, 2003. 8745
- Rossa, A., Liechti, K., Zappa, M., Bruen, M., Germann, U., Haase, G., Keil, C., and Krahe, P.: The COST 731 Action: a review on uncertainty propagation in advanced hydro-meteorological forecast systems, Atmos. Res., 100, 150–167, doi:10.1016/j.atmosres.2010.11.016, 2011. 8745
- Toth, M., Jones, E., Pittman, D., and Solomon, D.: DOW radar observations of wind farms, B. Am. Meteorol. Soc., 92, 987–995, doi:10.1175/2011BAMS3068.1, 2011. 8746
- Vogt, R. J., Crum, T. D., Greenwood, W., Ciardi, E. J., and Guenther, R. G.: New criteria for evaluating wind turbine impacts on NEXRAD radars, in: Proceedings of WINDPOWER 2011, Anaheim, CA, United States, American Wind Energy Association, 2011. 8745, 8750

Wind turbines and Doppler weather radars

L. Norin

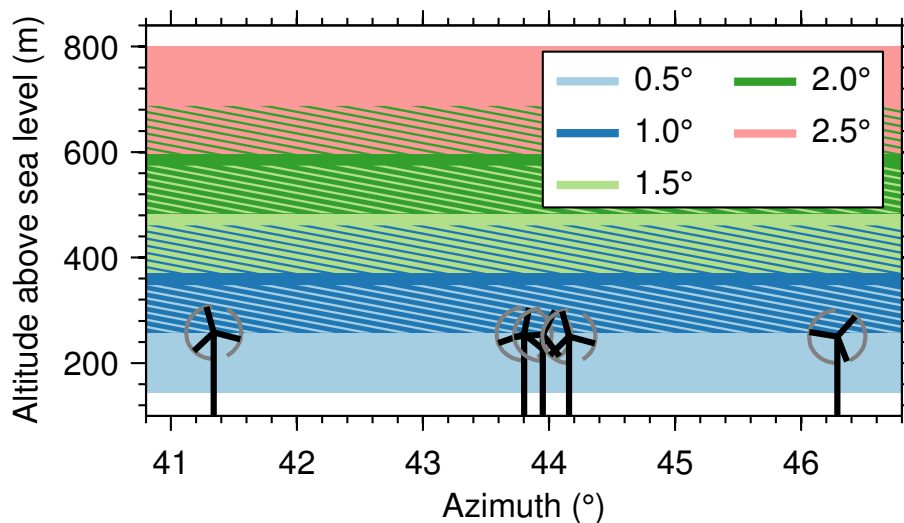


Figure 1. Schematic plot of Brunsmo wind farm. The positions and heights of the wind turbines are shown together with the altitudes of the half-power beam width of the main radar lobe for five lowest tilt angles ($0.5^\circ \leq \theta \leq 2.5^\circ$) at the wind farm.

[Title Page](#)[Abstract](#)[Introduction](#)[Conclusions](#)[References](#)[Tables](#)[Figures](#)[◀](#)[▶](#)[◀](#)[▶](#)[Back](#)[Close](#)[Full Screen / Esc](#)[Printer-friendly Version](#)[Interactive Discussion](#)

Wind turbines and Doppler weather radars

L. Norin

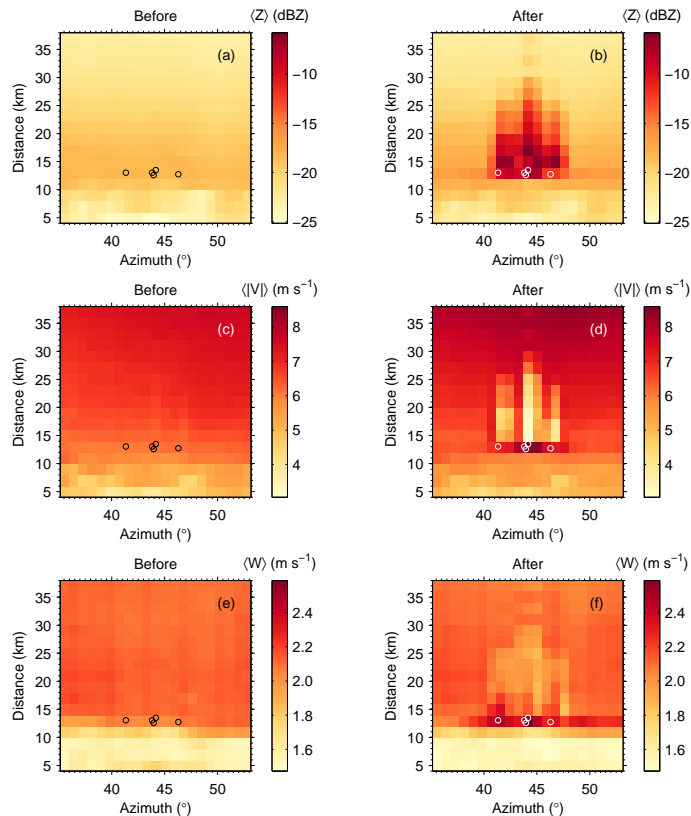


Figure 2. Average reflectivity $\langle Z \rangle$, average absolute radial velocity $\langle |V| \rangle$, and average spectrum width $\langle W \rangle$, before and after the construction of Brunsmo wind farm. The locations of the wind turbines are shown with black or white circles. The impact of the wind turbines is seen for all spectral moments as changes to their average value. The impact of the wind turbines extends to radar cells both cross- and downrange from the wind farm.

Title Page

Abstract

Introduction

Conclusions

References

Tables

Figures

◀

▶

◀

▶

Back

Close

Full Screen / Esc

Printer-friendly Version

Interactive Discussion



Wind turbines and Doppler weather radars

L. Norin

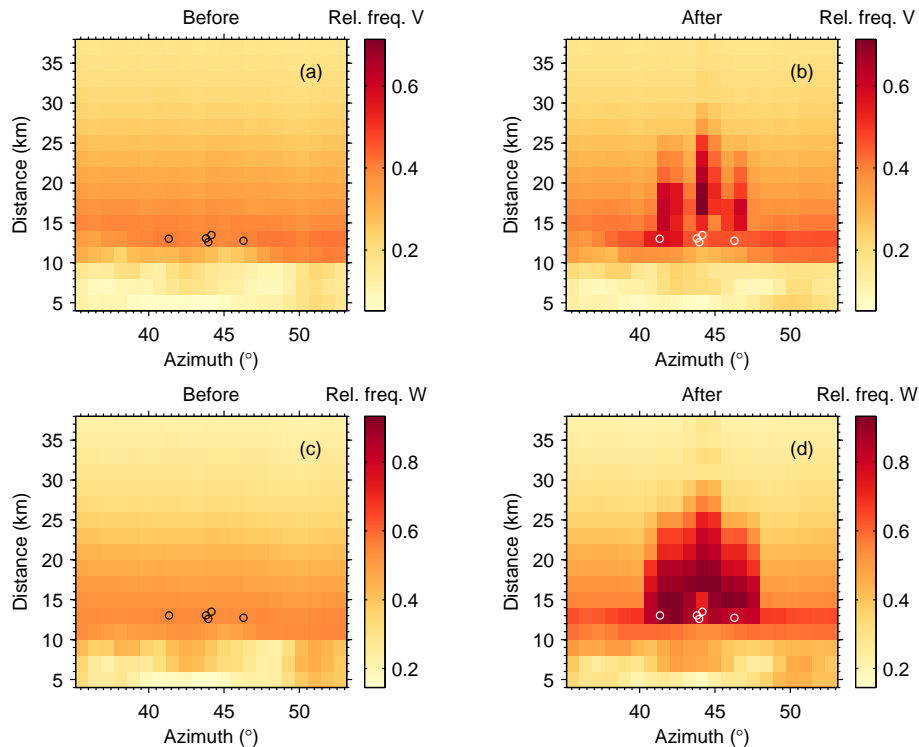


Figure 3. Relative frequency of real (detected and valid) measurements of radial velocity V and spectrum width W , before and after the construction of Brunsmo wind farm. The locations of the wind turbines are shown with black or white circles. The wind turbines are seen to increase the frequency of real measurements of V and W , both at the location of the wind turbines as well as cross- and downrange from the wind farm.

Wind turbines and
Doppler weather
radars

L. Norin

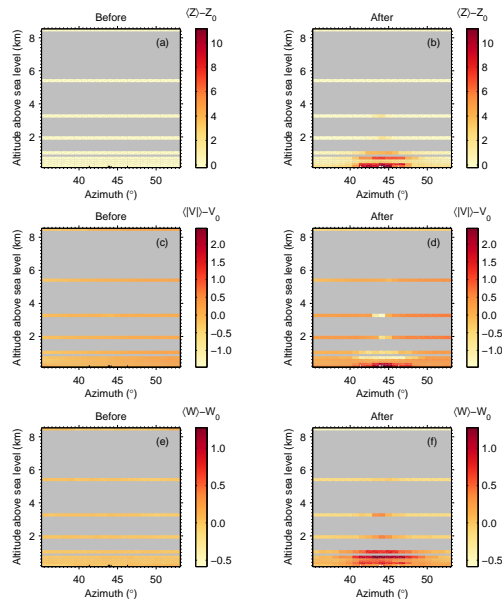


Figure 4. Difference in average reflectivity, $\langle Z \rangle - Z_0$, difference in average absolute radial velocity, $\langle |V| \rangle - V_0$, and difference in average spectrum width, $\langle W \rangle - W_0$, for all tilt angles ($0.5^\circ \leq \theta \leq 40^\circ$), before and after the construction of Brunsmo wind farm. For each scan, Z_0 , V_0 , and W_0 were calculated as the mean value in azimuth (for the azimuth gates shown in the figure) of the corresponding spectral moment, before the construction of the wind farm. For every scan, the data shown were taken from the range bin corresponding to the location of the wind turbines. For scans with higher tilt angles ($2.5^\circ \leq \theta \leq 40^\circ$) the average values of the two range bins nearest the wind turbines were used since for these scans the range resolution is two times that of the scans with lower tilt angles. The locations of the wind turbines are shown on the bottom of each plot as black or white vertical lines. The wind turbines are in radar line-of-sight for the scans with the two lowest tilt angles but are nevertheless seen to have an impact on scans with higher tilt angles.

Title Page

Abstract

Introduction

Conclusions

References

Tables

Figures



Back

Close

Full Screen / Esc

Printer-friendly Version

Interactive Discussion



Wind turbines and Doppler weather radars

L. Norin

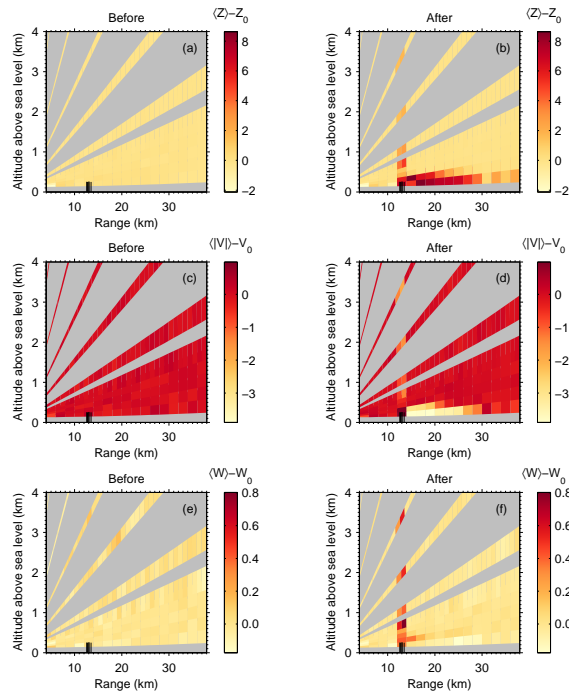


Figure 5. Difference in average reflectivity, $\langle Z \rangle - Z_0$, difference in average absolute radial velocity, $\langle |V| \rangle - V_0$, and difference in average spectrum width, $\langle W \rangle - W_0$, for all tilt angles ($0.5^\circ \leq \theta \leq 40^\circ$), before and after the construction of Brunsmo wind farm. For each scan, Z_0 , V_0 , and W_0 were calculated as the mean value in azimuth (for the azimuth gates shown in Fig. 4) of the corresponding spectral moment, before the construction of the wind farm. Data were taken from azimuth gate 52, the gate in which three wind turbines are located (near 44° azimuth). The locations of the wind turbines are shown on the bottom of each plot as black vertical lines. The wind turbines are in radar line-of-sight for the scans with the two lowest tilt angles but are nevertheless seen to impact scans with higher tilt angles.

Title Page

Abstract

Introduction

Conclusions

References

Tables

Figures



Back

Close

Full Screen / Esc

Printer-friendly Version

Interactive Discussion



Wind turbines and Doppler weather radars

L. Norin

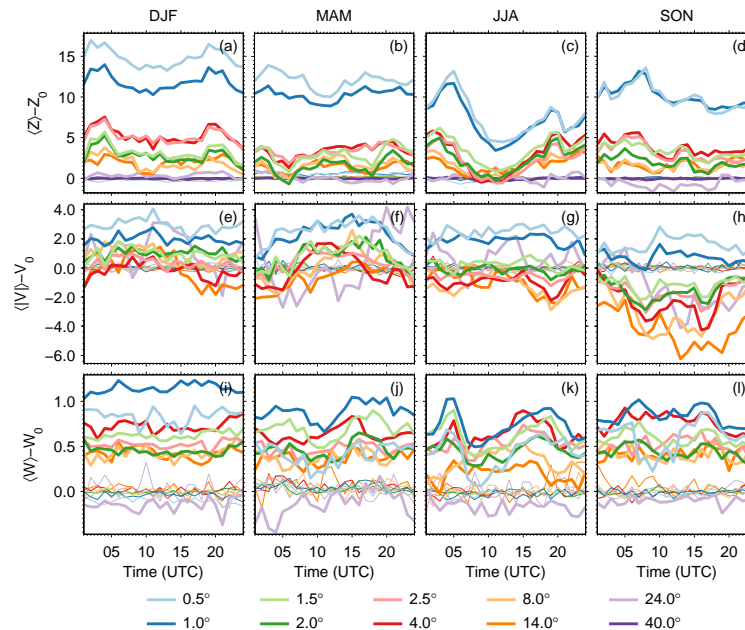


Figure 6. Difference in average reflectivity, $\langle Z \rangle - Z_0$, difference in average absolute radial velocity, $\langle |V| \rangle - V_0$, and difference in average spectrum width, $\langle W \rangle - W_0$, for a radar cell in which three wind turbines are located for all tilt angles ($0.5^\circ \leq \theta \leq 40^\circ$), before (thin lines) and after (thick lines) the construction of Brunsmo wind farm, as a function of season and time of day. For each scan, Z_0 , V_0 , and W_0 were calculated as the mean value in azimuth (for the azimuth gates shown in Fig. 4) of the corresponding spectral moment, before the construction of the wind farm. Variations in the spectral moments are partly attributed to changes in atmospheric refraction. During winter (DJF), temperature inversions are common over Sweden leading to increased amplitudes in the spectral moments, regardless of the time of day. During the warm season temperature inversions are most common during early morning, producing a peak in amplitude. The peak in the afternoon, most clearly seen during summer (JJA), is attributed to a rapid decrease in water vapour content with height.

Title Page

Abstract

Introduction

Conclusions

References

Tables

Figures



Back

Close

Full Screen / Esc

Printer-friendly Version

Interactive Discussion



Wind turbines and Doppler weather radars

L. Norin

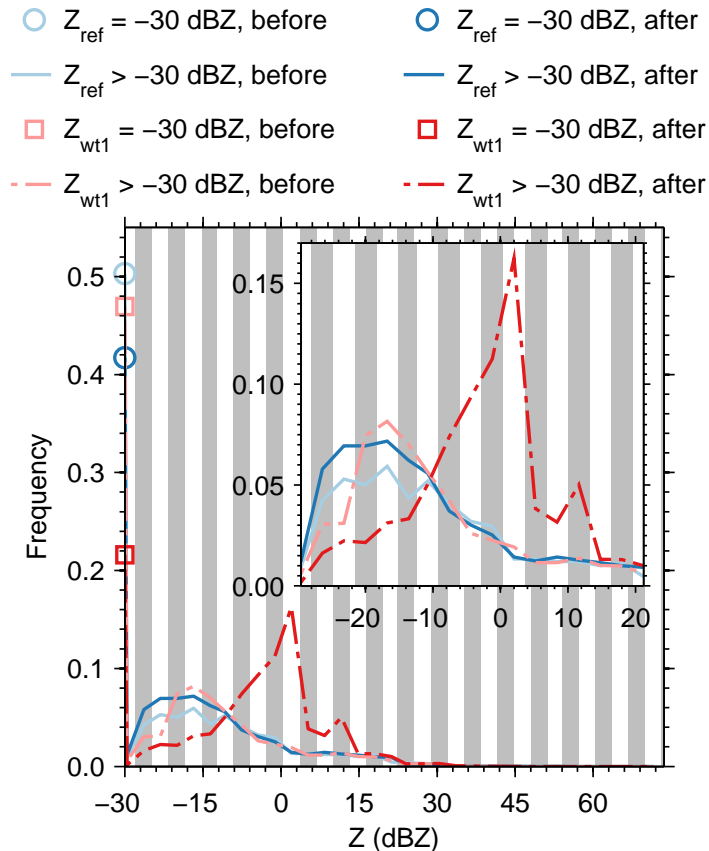


Figure 7. Relative frequency distributions of reflectivity from a reference radar cell, Z_{ref} , and from a radar cell in which three wind turbines are located, Z_{wt} , before and after the construction of a wind farm, using data from the scan with the lowest tilt angle ($\theta = 0.5^\circ$). The grey and white backgrounds represent the bins that were used to create the distributions.

Title Page

Abstract

Introduction

Conclusions

References

Tables

Figures



Back

Close

Full Screen / Esc

Printer-friendly Version

Interactive Discussion



Wind turbines and
Doppler weather
radars

L. Norin

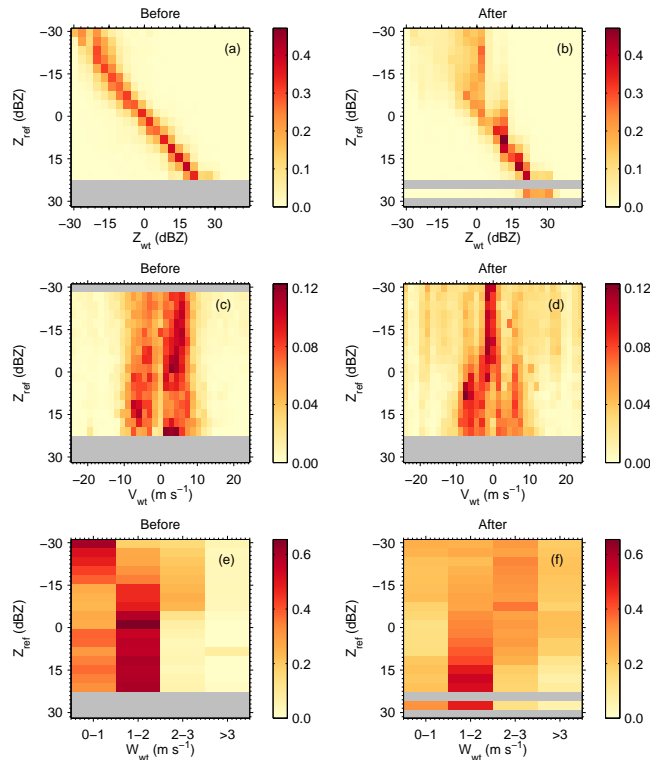


Figure 8. Relative frequency distributions of reflectivity, Z_{wt} , radial velocity, V_{wt} , and spectrum width, W_{wt} , from a radar cell in which three wind turbines are located as a function of reflectivity from a reference radar cell, Z_{ref} , using data from the scan with the lowest tilt angle ($\theta = 0.5^\circ$). Panels on the left-hand side (**a**, **c** and **e**) show relative frequency distributions before the wind farm was constructed and panels to the right (**b**, **d** and **f**) show the corresponding distributions after the wind farm start-of-operations. For $Z_{ref} \gtrsim 5$ dBZ the distributions of Z_{wt} , V_{wt} , and W_{wt} are similar before and after the construction of the wind farm. However, for $Z_{ref} \lesssim 5$ dBZ the distributions before and after the construction of the wind farm look different.

Wind turbines and Doppler weather radars

L. Norin

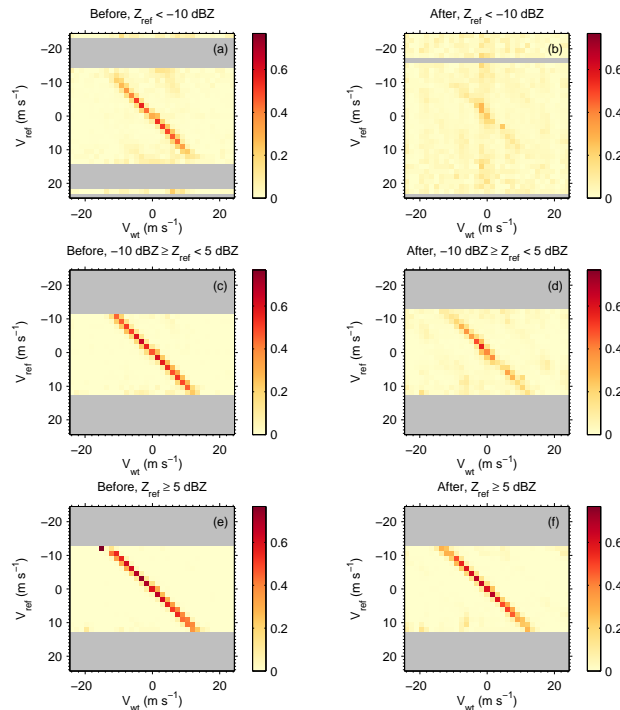


Figure 9. Relative frequency distributions of radial velocity from a radar cell in which three wind turbines are located, V_{wt} , as a function of radial velocity, V_{ref} , and reflectivity, Z_{ref} , from a reference radar cell. Data were taken from the scan with the lowest tilt angle ($\theta = 0.5^\circ$). Panels on the left-hand side (**a**, **c** and **e**) show relative frequency distributions of V_{wt} for $Z_{ref} < -10$ dBZ, -10 dBZ $\geq Z_{ref} < 5$ dBZ, and $Z_{ref} \geq 5$ dBZ, respectively, before the construction of the wind farm. Panels on the right-hand side (**b**, **d** and **f**) show the corresponding distributions, using data obtained after the construction of the wind farm. In (**b**), for $Z_{ref} < -10$ dBZ, almost no correlation exists between V_{wt} and V_{ref} but it is clear that the correlation recovers for increasing values of Z_{ref} (**d** and **f**).

[Title Page](#)
[Abstract](#)
[Introduction](#)
[Conclusions](#)
[References](#)
[Tables](#)
[Figures](#)
[◀](#)
[▶](#)
[◀](#)
[▶](#)
[Back](#)
[Close](#)
[Full Screen / Esc](#)
[Printer-friendly Version](#)
[Interactive Discussion](#)

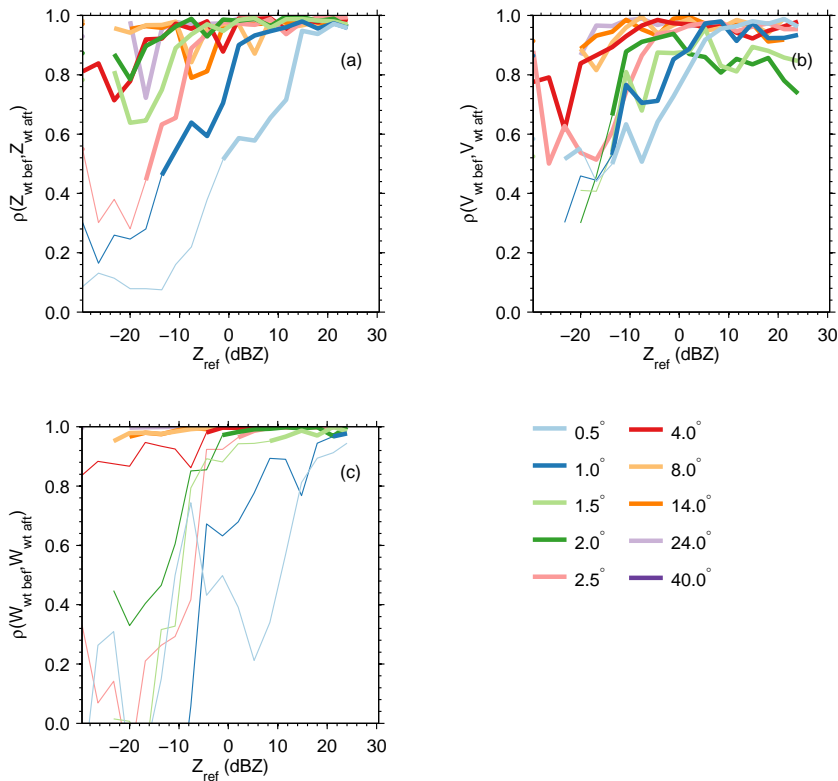



Figure 10. Correlation coefficients, ρ , between frequency distributions of spectral moments from a wind turbine-affected radar cell before ($Z_{wt\ bef}$, $V_{wt\ bef}$, and $W_{wt\ bef}$) and after ($Z_{wt\ aft}$, $V_{wt\ aft}$, and $W_{wt\ aft}$) the construction of Brunsmo wind farm, as a function of reflectivity from a reference radar cell, Z_{ref} , for all tilt angles. The correlation of the spectral moments recover for higher values of Z_{ref} (increasing influence of the weather signal) and for higher tilt angles (decreasing influence of the wind farm). Correlations significant on $p < 0.05$ -level are drawn with thick lines.